PERFORMANCE EVALUATION AND HILS TEST OF CONTROL ALLOCATION METHODS FOR RECONFIGURATION CONTROL

Byoung-Mun Min*, Bong-Ju Kim, Eung-Tai Kim***, and Min-Jea Tahk***

* Korea Advanced Institute of Science and Technology (KAIST)

** Korea Aerospace Industry (KAI)

*** Korea Aerospace Research Institute (KARI)

Keywords: *Control Allocation Methods, Reconfiguration Control, HILS Test*

Abstract

This paper focuses on the performance evaluation of several control allocation methods for reconfiguration control of UAV with redundant control surfaces. Control allocation scheme can be implemented into the flight control system via two step design procedure. The first step is to design a baseline control system for an aircraft under the assumption that all control surfaces are normally operated. The second step is to design a control allocation algorithm that maps the total control command generated by baseline flight control system on each control surface. In this paper, several control allocation algorithms such as Pseudo-inverse (PCA) method, Direct (DCA) method, and Optimization-based (OCA) method are implemented and integrated into the baseline flight control system of DURUMI-II UAV. The performances of these several control allocation algorithms are evaluated by simulation study. Also, HILS (Hardware-In-the-Loop-Simulation) test is performed to verify the capability of the real-time implementation of reconfiguration control scheme based on control allocation algorithm to UAV system.

1 Introduction

Modern aircraft systems including several UAVs have redundant control surfaces to obtain the high maneuverability and performance or to increase the safety against unexpected failure or damage of some control surfaces. Also, X-36, X-45, and BWB(Blended Wing-Body) UAV, which show the revolutionary configurations, may be controlled in a different way compared to the conventional types of aircraft. In the conventional aircraft, each control surface, i.e. elevator, aileron, and rudder, independently generates the demanded control moments in pitch, roll, and yaw directions. However, in the control of over-actuated or non-conventional aircraft, the most important problem is how to effectively generate the required moments by distributing the control signals, which are produced from flight control law of aircraft, to each individual control surface.

Since the early 1990s, various control allocation algorithm has been widely studied. The control allocation problem, in general, can be formulated as a form of the constrained optimization problem. Pseudo-inverse method was proposed to find the control input that minimizes the control power or the error between the desired moment and the generated moment satisfying the control limits [1-3]. Another method is one of the non-optimal scheme called as daisy chain control allocation [4,5]. In this approach, the control input is calculated by multiple steps such a way of, firstly, grouping the control inputs and sequentially actuating each control group until the desired moment is generated or all control groups are deflected to their limits. The closed-form solutions of a generalized inverse and daisy chain method are shown and their performance is compared in Ref. [6]. Durham suggested a direct control allocation scheme [7, 8]. Since the direct control allocation selects the control input of each control effector based on the geometric reasoning, this algorithm requires a heavy computation time. Harkegard solved the

constrained control allocation problem by using an active set algorithm and backstepping technique [9, 10]. However, unfortunately, the most of the previous researches relating to control allocation problem do not considered the performance of flight control system. In other word, the proposed control allocation schemes are mainly restricted to the point of the control command distribution. It is possible to degrade its performance when the proposed schemes are implemented to the real system.

This paper focuses on the evaluation of the performance of several control allocation logics under the condition that it is integrated with the flight control law of UAV. Furthermore, HILS test is performed to investigate its real-time applicability. This paper is organized as follows. Section 2 addresses the generalized control allocation problem and some control allocation schemes considered in this paper. The UAV platform and its baseline control law are described in Section 3. Nonlinear simulation results for reconfiguration control applying the implemented control allocation algorithms and HILS test system and its results are shown in Section 4. Section 5 concludes.

2 Generalized Control Allocation Problem & Several Control Allocation Algorithms

There are several ways to express a control allocation problem. In this section, we introduce the generalized control allocation problem for an over-actuated system with some control input constraint.

2.1 Generalized Control Allocation Problem

In general, control allocation problem is to find the mapping function that distributes the demanded control commands to each actuator as following expression.

$$g\left(u(t)\right) \;=\; v(t) \qquad (1)$$

where $v(t) \in \mathbf{R}^n$ is the virtual control input generated by control law and $u(t) \in \mathbf{R}^m$ is the true control input to operate control actuators. Also, $g:\mathbf{R}^m \rightarrow \mathbf{R}^n$ is nonlinear mapping function. In an over-actuated system, m is always larger than n. For the linear system, Eq. (1) can be written as

$$B\,u(t) \;=\; v(t) \qquad (2)$$

where $B \in \mathbf{R}^{n\times m}$ is the control effectiveness matrix which is inherently determined from the role of control surfaces in aircraft system. Here, each control surface has lower and upper bounds, i.e. $\underline{u}$ and $\overline{u}$, caused by position and slew rate limits of mechanical actuators.

$$\underline{u}_i \;\le\; u_i \;\le\; \overline{u}_i\,, \quad for \quad i = 1,\, 2,\, \cdots,\, m \qquad (3)$$

Eqs. (2) and (3) are called the generalized constrained control allocation problem for linear system.

2.2 Pseudo-inverse Control Allocation (PCA)

The Solution of control allocation problem expressed in Eqs. (2) and (3) can be obtained by solving the constrained optimization problem written in Eq. (4).

$$\begin{aligned} &\underset{u}{\text{minimize}} \quad J \;=\; \|u\|_2^2 \\ &subject \quad to \quad B\,u = v \quad , \quad \underline{u} \le u \le \overline{u} \end{aligned} \qquad (4)$$

If all of the inequality constraints are inactive, the optimal solution of Eq. (4) can be calculated by the following equation

$$u \;=\; B^{\dagger} v \qquad (5)$$

where $B^{\dagger} = B^T \left(BB^T\right)^{-1}$ is a right pseudo-inverse.

This approach is very simple and fast, however, it can not explicitly treat the inequality constraint on control input. A weighted pseudo-inverse method was suggested by Snell et al. [11] to obtain a feasible solution under the condition of control limits.

2.3 Direct Control Allocation (DCA)

DCA was introduced by Durham [7] at 1993. In this approach, the actual control input which is the real signal to actuate the control surface was uniquely chosen by the geometric inference composed of the subset of the constrained controls and their image on moment space. This method guarantees that the maximum control

moment is generated in the feasible region. The procedure to determine the actual control input in this approach can be summarized as follows:. If the virtual control input v is produced by the control law of aircraft, firstly, a feasible control input u^*, which is a control input with the maximum magnitude coincident with the direction of the virtual control input vector, is calculated. Here, a new virtual control input $v^* = Bu^*$ is obtained. The actual control input u is finally determined as

$$u = \begin{cases} \frac{1}{a} u^*, & if \quad a > 1 \\ u^*, & if \quad a < 1 \end{cases} \tag{6}$$

where the constant a is the ratio of v and v^* defined by L-2 norm. Referring to Bodson [1], the above procedure can be redefined as the following constrained optimal problem

$$\begin{aligned} &\underset{a,\,u}{\text{maximize}} \quad a \\ &\textit{subject to} \quad Bu = av, \quad \underline{u} \le u \le \bar{u} \end{aligned} \tag{7}$$

2.4 Optimization-based Control Allocation (OCA)

Harkegard [9] suggested an OCA to solve dynamic control allocation problem using active set algorithm. In this method, the actual control input u is selected by solving the following two-step optimization problem

$$\begin{aligned} u &= \arg \min_{u \in \Omega} \left\| W_u (u - u_d) \right\|_2 \\ \Omega &= \arg \min_{\underline{u} \le u \le \bar{u}} \left\| W_v (Bu - v) \right\|_2 \end{aligned} \tag{8}$$

where u_d, W_u, and W_v, respectively, denote the desired control input and weighting matrices. This algorithm finds only one solution in the sense of optimality if there exist multiple solutions, whereas, if there is no exact solution, it chooses the best solution that approximates the virtual control input v as close as possible.

3 UAV Platform & Its Baseline Flight Control System

3.1 UAV Platform

DURUMI-II UAV developed by Korea Aerospace Research Institute was adopted to a vehicle platform. Its configuration and some physical parameters are shown in Fig. 1 and Table 1, respectively. As depicted in Fig.1, its main control surfaces are split into the right and left pairs and, moreover, all control surfaces can be independently actuated. For example, the right and left ailerons are deflected in the same direction or in the opposite direction such as flaperon. Eventually, the control effectiveness matrix B of DURUMI-II UAV is inherently determined as Eq. (9).

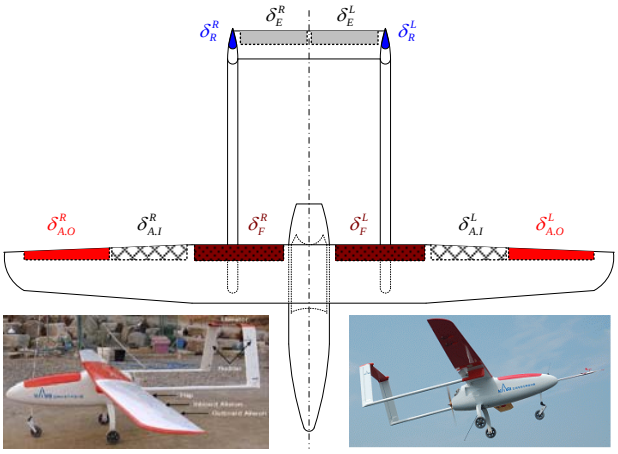

Fig. 1. Configuration and control surfaces of DURUMI-II UAV

Table 1. Some physical parameters of DURUMI-II UAV

Fuselage Length (m)		2.7
Engine Power (hp)		7.9
Speed (km/h)	Stall	55.0
	Maximum	120.0
	Cruising	100.0
Weight (kg)	Empty	22.0
	Max. Take-off	37.0
Moment of Inertia (kg·m^2)	I_{xx}	18.13
	I_{yy}	13.10
	I_{zz}	22.29
Wing Area (m^2)	Main Wing	1.52
	Horizontal Tail	0.12
	Vertical Tail	0.27
Wing Span (m)	Main Wing	4.80

$$B = \begin{bmatrix} 0.315 & 0.315 & 0.019 & 0.019 & 0.014 & 0.014 & 0.014 & 0.014 & 0.000 & 0.000 \\ 0.000 & 0.000 & 0.148 & -0.148 & 0.183 & -0.183 & 0.152 & -0.152 & 0.021 & -0.021 \\ 0.000 & 0.000 & 0.008 & -0.008 & 0.012 & -0.012 & 0.011 & -0.011 & 0.162 & 0.162 \end{bmatrix} \quad (9)$$

$$u = \begin{bmatrix} \delta_e^L & \delta_e^R & \delta_f^L & \delta_f^R & \delta_{i.a}^L & \delta_{i.a}^R & \delta_{o.a}^L & \delta_{o.a}^R & \delta_r^L & \delta_r^R \end{bmatrix}^T$$

$$\underline{u}\ (or\ \bar{u}) = \begin{bmatrix} \pm 20 & \pm 20 & \pm 30 & \pm 30 & \pm 30 & \pm 30 & \pm 30 & \pm 30 & \pm 10 & \pm 10 \end{bmatrix} (\text{deg})$$

where superscripts *R* and *L* indicate the right and left surfaces and subscripts *e, f, i.a, o.a,* and r denote, respectively, elevator, flap, inboard and outboard ailerons, and rudder.

3.2 Baseline Flight Control System

The baseline flight control system of DURUMI-II UAV is composed of speed and altitude hold controller for longitudinal motion and heading orientation controller for lateral-directional motion as shown in Fig. 2. Altitude hold and heading orientation autopilot is constituted of inner-loop controllers for roll and pitch stabilization and orientation. The baseline flight control system was designed under the assumption that all control surfaces are operated normally. As shown in Fig. 2, altitude and heading angle are controlled by elevator and inboard and outboard ailerons. Rudder plays a role of suppressing the sideslip angle during lateral maneuver and total speed is controlled by throttle of engine.

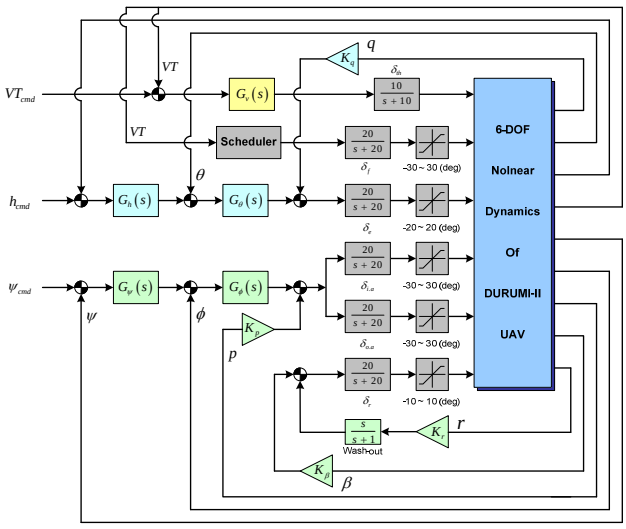

Fig. 2. The baseline flight control system of DURUMI-II UAV

Controllers included in longitudinal and lateral-directional autopilot shown in Fig. 2 are given in Table 2.

Table 2. Some physical parameters of DURUMI-II UAV

Speed Controller	$G_V(s) = \dfrac{0.03s + 0.002}{s}$
Pitch SAS	$K_q = 0.01$
Pitch Controller	$G_\theta(s) = \dfrac{(5s+0.5)(s+0.5)}{s(s+0.05)}$
Altitude Controller	$G_h(s) = 0.4$
Yaw SAS and Sideslip Suppressor	$K_r = 0.5$
	$K_\beta = 0.2$
Roll SAS	$K_p = 0.01$
Roll Controller	$G_\phi(s) = 10$
Heading Controller	$G_\psi(s) = 0.2$

As illustrated in Fig. 3, control allocation algorithm explained in Section 2 was integrated to the baseline flight control system shown in Fig. 2. Here, only altitude hold and heading orientation autopilot loops are merged into control allocation algorithm and speed hold autopilot loop was independently operated.

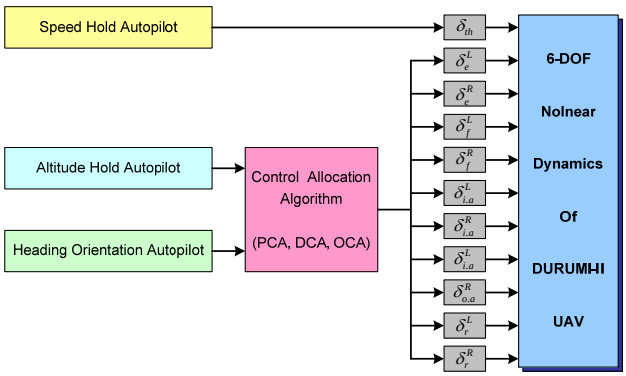

Fig. 3. Flight control system integrated with baseline control law and control allocation algorithm

Fig. 4 shows the control performance of the baseline control system of DURUMI-II UAV.

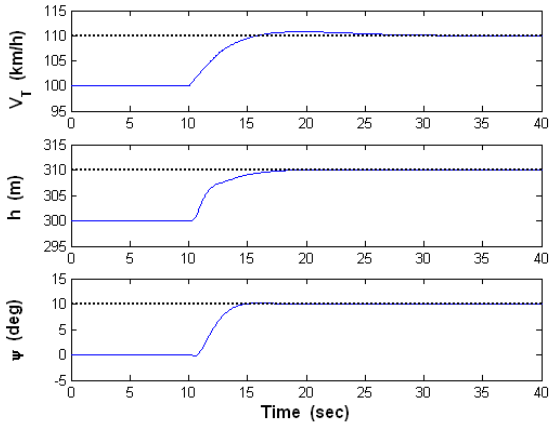

Fig. 4. Control performance of the baseline flight control system of DURUMI-II UAV

4 Simulation and HILS Test Results

In this section, firstly the performance of reconfiguration control based on the control allocation technique is evaluated via nonlinear simulation. Also, HILS (Hardware-In-the-Loop Simulation) test was performed to verify the possibility of the real-time implementation.

4.1 Simulation Results

The fault detection and isolation (FDI) problem is not treated in this paper, since the main objective of this paper is to evaluate the performance of reconfiguration control based on control allocation algorithms. Therefore, we assume that FDI process is perfectly completed within 1*sec* and reconfiguration control system (RCS) is executed after 1*sec* of fault. Figs. 5 and 6 show the flight trajectories of the nominal model, fault model controlled by only the baseline control system, and fault model controlled by RCS, respectively. In this nonlinear simulation, we assume that right inboard aileron $\delta_{i.a}^{R}$, left outboard aileron $\delta_{o.a}^{L}$, and right rudder δ_{r}^{R} are simultaneously stuck at the deflected position of, respectively, +15 *deg*, -15 *deg*, and +5 *deg* during the glide approach phase. As shown in Fig. 5, since the baseline control system cannot effectively eliminate the moment generated by the faulty control surfaces, the fault model without RCS is hard to achieve the control objective. However, as shown in Figs. 6 ~ 10, if the RCS is applied, healthy ailerons are deflected to the same sides and rudder is deflected to the opposite side of each pair of their faulty surfaces to reduce the unexpected moment effect and the additional moment for lateral maneuver is generated by actuating one pair of flap. Here, we observe that the results of PCA and OCA are very similar to each other. The reason is that PCA, not violating the constraints, provides the minimum norm solution. Also, PCA algorithm may be implemented to the real-time system because of its computational time is fast enough.

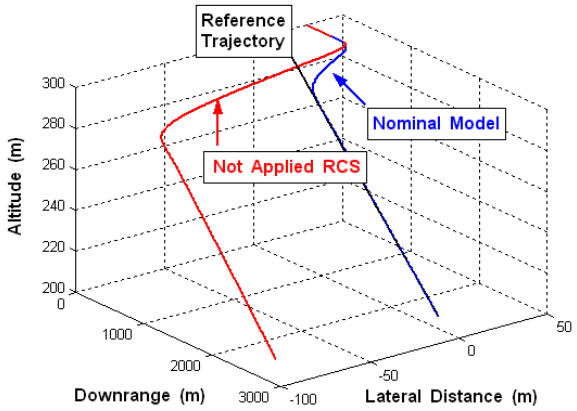

Fig. 5. Trajectories of nominal model and fault model without RCS

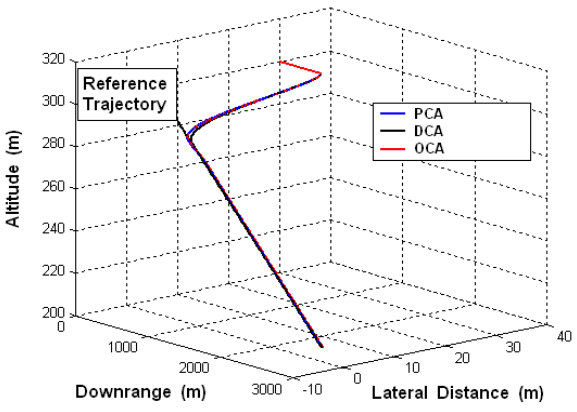

Fig. 6. Trajectories of PCA, DAC, and OCA

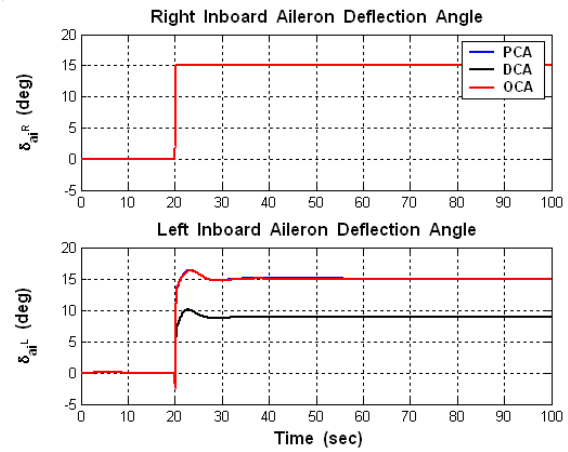

Fig. 7. Time histories of inboard aileron deflection angle

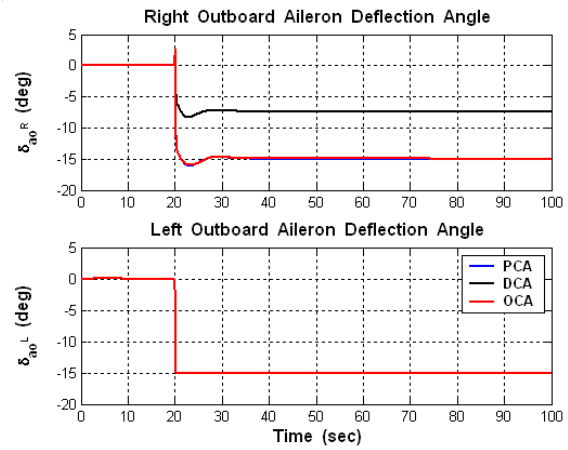

Fig. 8. Time histories of outboard aileron deflection angle

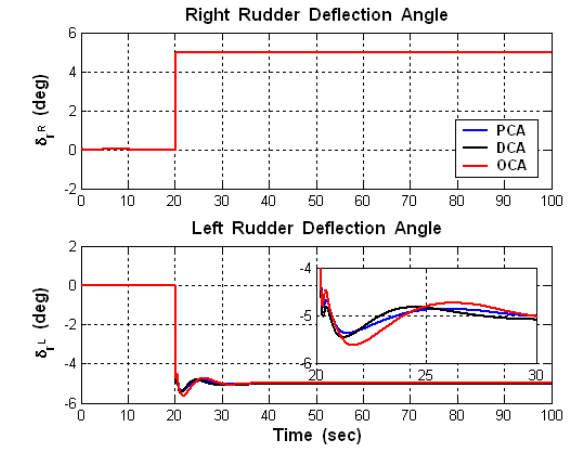

Fig. 9. Time histories of rudder deflection angle

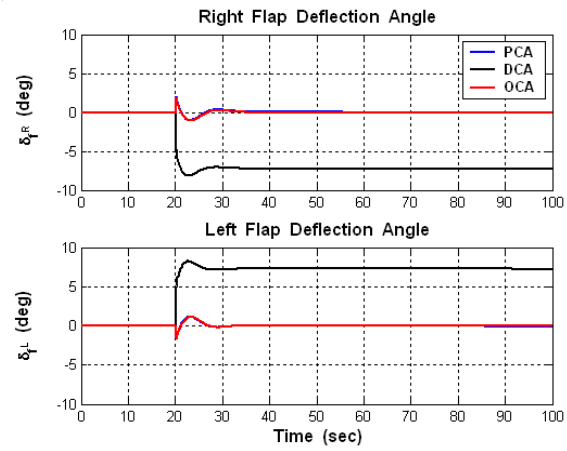

Fig. 10. Time histories of flap deflection angle

4.2 HILS Test Results

Based on the analysis results of nonlinear simulation, we performed HILS test to verify the possibility of real-time implementation. PCA algorithm was adopted for HILS test of RCS. Fig. 11 illustrates the configuration of HILS system. HILS system is composed of flight control computer (FCC), servo motor module, virtual aircraft computer, and visual computer. FCC and servo motor included in HILS system are the identical model equipped in UAV. Virtual aircraft computer represents the flight motion based on the mathematical model of UAV instead of a real vehicle. Flight data generated by virtual aircraft computer are transmitted to FCC in the same signal format of navigation sensors as depicted in Fig. 11.

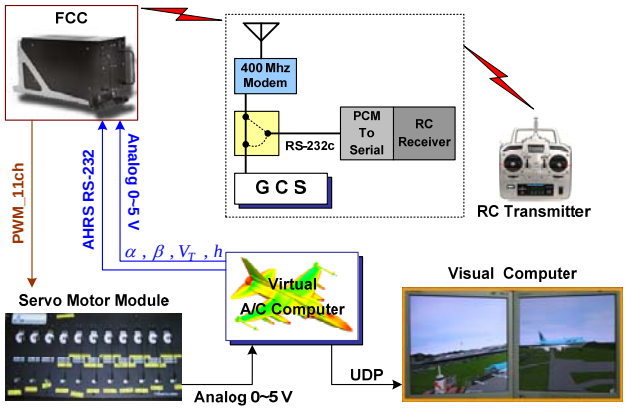

Fig. 11. Configuration of HILS system

Figs. 12 ~ 16 show the HILS test result of RCS for DURUMI-II UAV. HILS test was performed under the flight scenario that left inboard aileron $\delta_{i.a}^{L}$ and right outboard aileron $\delta_{o.a}^{R}$ are stuck at +5 *deg* and -10 *deg* when the UAV flies in the steady-state level flight maintaining the altitude of 100 *m* and the velocity of 100 *km/h*, respectively. Here, RCS mode is engaged after 2 *sec* of fault in control surfaces. As shown in Fig 13, UAV recovers its attitude angles for the steady-state level flight as soon as the RCS mode is engaged. The healthy control surfaces, i.e. right inboard aileron $\delta_{i.a}^{R}$ and left outboard aileron $\delta_{o.a}^{L}$, are deflected in the same position of the faulty control surfaces. As the results of RCS, the unexpected moment caused by the faulty control surfaces is properly eliminated.

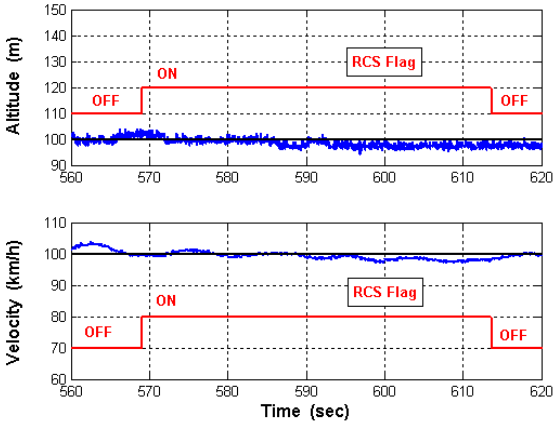

Fig. 12. Time histories of altitude and velocity

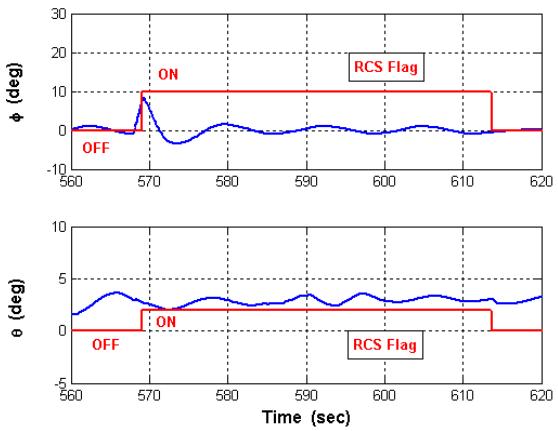

Fig. 13. Time histories of roll and pitch attitude angles

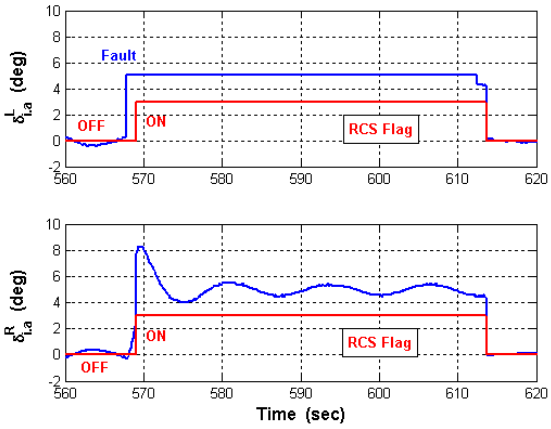

Fig. 14. Time history of inboard aileron deflection angle

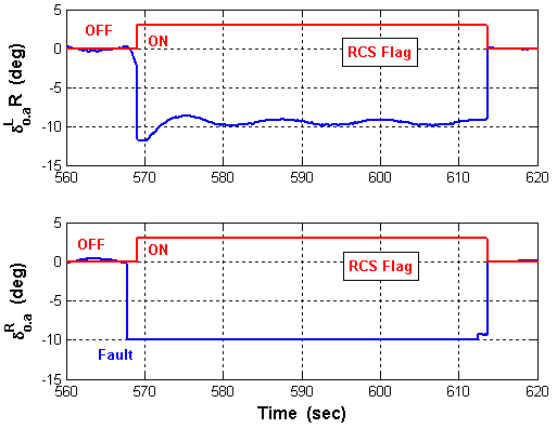

Fig. 15. Time history of outboard aileron deflection angle

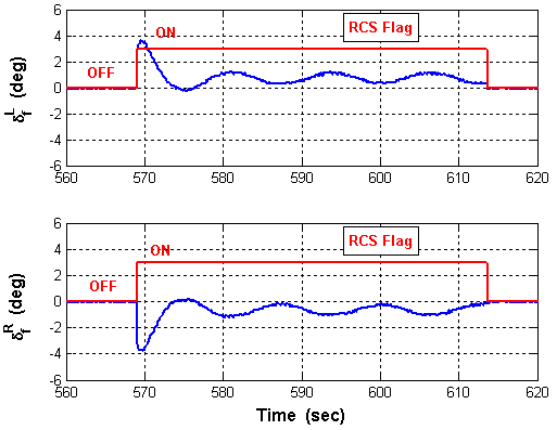

Fig. 16. Time history of flap deflection angle

5 Conclusions

In this paper, we evaluated the performance of the reconfiguration control system for UAV. PCA, DCA, and OCA algorithms are developed in the RCS of DURUMI-II UAV and their performance and characteristics are investigated through nonlinear simulation with fault scenario. HILS test for RCS of UAV was performed to verify the real-time implementation. From the nonlinear simulation and HILS test results, we concluded that RCS based on PCA algorithm shows a satisfactory performance and it might be implemented into the real-time system.

References

[1] Bodson, M., Evaluation of Optimization Methods for Control Allocation, *Journal of Guidance, Control, and Dynamics*, Vol. 25, No. 4, pp 703-711, 2002.

[2] Virnig, J. C. and Bodden, D. S., Multivariable Control Allocation and Control Law Conditioning When Control Effectors Limit, *AIAA Guidance, Navigation, and Control Conference and Exhibit*, Scottsdale, AZ, 1994.

[3] Jin, J., Modified Pseudoinverse Redistribution Methods for Redundant Controls Allocation, *Journal of Guidance, Control, and Dynamics*, Vol. 28, No. 5, pp 1076-1079, 2005.

[4] Berg, J. M., Hammet, K. D., Schwartz, C. A., and Banda, S. S., An Analysis of the Destabilizing Effect of Daisy Chained Rate-limited Actuators, *IEEE Transactions on Control Systems Technology*, Vol. 4, No. 2, pp 171-176, 1996.

[5] Buffington, J. M. and Enns, D. F., Lyapunov Stability Analysis of Daisy Chain Control Allocation, *Journal of Guidance, Control, and Dynamics*, Vol. 19, No. 6, pp 1226-1230, 1996.

[6] Bordignon, K. A. and Durham, W. C., Closed-Form Solution to Constrained Control Allocation Problem, *Journal of Guidance, Control, and Dynamics*, Vol. 18, No, 5, pp 1000-1007, 1995.

[7] Durham, W. C., Constrained Control Allocation, *Journal of Guidance, Control, and Dynamics*, Vol. 16, No. 4, pp 717-725, 1993.

[8] Durham, W. C., Constrained Control Allocation: Three-Moment Problem, *Journal of Guidance, Control, and Dynamics*, Vol. 17, No. 6, pp 1371-1373, 1994.

[9] Harkegard, O., Efficient Active Set Algorithms for Solving Constrained Least Square Problems in Aircraft Control Allocation, *Proceedings of the 41th IEEE Conference on Decision and Control*, Las Vegas, NV, pp 1295-1300, 2002.

[10] Harkegard, O., *Backstepping and Control Allocation with Applications to Flight Control*, Ph. D Thesis, Linkoping Univ. Sweden, 2003.

[11] Snell, S. A., Enns, D. F., and Garrard Jr., W. L., Nonlinear inversion flight for a supermaneuverable aircraft, *Journal of Guidance, Control, and Dynamics*, Vol. 5, No. 4, pp 976-984, 1992.

Copyright Statement